

ASME Journal of Offshore Mechanics and Arctic Engineering Online journal at:

https://asmedigitalcollection.asme.org/offshoremechanics



Franciska Müller

Institute for Ship Structural Design and Analysis,
Hamburg University of Technology,
21073 Hamburg, Germany
e-mail: franciska.mueller@tuhh.de

Jan Willem van Bergen

Ministry of Defense, Command Material and IT (COMMIT), Maritime Systems Department (AMS), 3584 AB Utrecht, Netherlands e-mail: postvoorJan@planet.nl

Mark A. Rodriguez

Naval Surface Warfare Center Carderock Division, Bethesda, MD 20817 e-mail: mark.a.rodriguez194.civ@us.navy.mil

Sander Dragt

Department of Naval and Offshore Structures, Netherlands Organization for Applied Scientific Research (TNO), 2629 JD Delft, Netherlands e-mail: sander.dragt@tno.nl

Franz von Bock und Polach

Institute for Ship Structural Design and Analysis, Hamburg University of Technology, 21073 Hamburg, Germany e-mail: franz.vonbock@tuhh.de

Sören Ehlers

German Aerospace Center (DLR), Institute of Maritime Energy Systems, 21502 Geesthacht, Germany e-mail: ehlers@tuhh.de

Finite Element Simulations of Ice Impacts on a Ship Hull Using the MCNS Model

In this study, ice floe impacts on a non-ice-strengthened ship structure are investigated using the finite element method (FEM) with the Mohr-Coulomb nodal split (MCNS) as an ice material model. With this analysis, we address three questions: How does the shape of the ice affect the impact? Is the location where the impact occurs significant? How does the direction of impact influence the loads experienced by the ship? The ice shapes used for this study are modeled based on previous experimental analyses and include round, flat-parallel, and sharp geometries. Impact locations considered are the plate field, bulkhead, and longitudinal stiffener, with impact directions of 0 deg (glancing impact), 30 deg, 60 deg, and 90 deg (perpendicular impact). The study compares load magnitude, plastic deformation, and strain energies across these scenarios to pinpoint significant influencing factors. Findings are compared against existing experimental and literature data, highlighting the critical impact parameters and identifying the worst-case scenario. The study indicates that all three parameters significantly affect the impact. Round and flat-parallel ice shapes result in higher loads compared to the sharp shape. The greatest deformations occur in the plate field and in the bulkhead impact locations. Additionally, the loads increase as the impact becomes more perpendicular.

[DOI: 10.1115/1.4069869]

Keywords: ship-ice interaction, FEM simulation, ice loads, offshore structures and ships in ice

1 Introduction and State-of-the-Art

As geopolitical interests and economic opportunities in the Arctic continue to grow, the region has seen a noticeable increase in ship traffic, particularly within the marginal ice zone. This area is characterized by dynamic and unpredictable ice conditions, posing substantial risks to maritime navigation, especially for vessels with low or no ice-class. When such ships navigate near the marginal ice zone, the risk of ice impact is significantly heightened. Consequently, it is crucial to understand the ice loads that non-ice-class ships can endure during collisions with ice features.

Ice collision forces on ships or structures can be estimated using the energy-based approach, which was first introduced by Popov et al. [1]. In this energy method, the force is limited by the available kinetic energy. The approach was later further developed by Daley [2], who extended it with the pressure-area model. The method proposed by Daley in 1999 has been applied to establish the ice load calculation in the unified requirements for polar ships by the International Association of Classification Societies (IACS). This method takes into account various ice geometries and impact locations (IL) and was later extended to include structural deformation [3]. The pressure-area curves underlying the IACS method typically address impacts involving relatively large contact areas. However, it is important to study impacts involving also small contact areas and to investigate the interaction effects when ice encounters stiff structural elements, such as webframes or bulkheads.

In this article, we investigate local ice impact loads on a non-ice-strengthened ship structure through full-scale finite element method (FEM) simulations. Due to the lightweight hull structure, the ship undergoes plastic deformation while the ice fails through crushing and spalling, resulting in the deformation energy being shared between the ice and the ship.

¹Corresponding author.

Contributed by the Ocean, Offshore, and Arctic Engineering Division of ASME for publication in the Journal of Offshore Mechanics and Arctic Engineering. Manuscript received March 18, 2025; final manuscript received September 9, 2025; published online October 1, 2025. Assoc. Editor: Jani Romanoff.

One of the challenges in this process is identifying an appropriate material model for the ice. Although several ice material models have been developed, as noted in Refs. [4–7], among others, only a handful of these FEM-based models have been applied to full-scale simulations.

Liu et al. [7] introduced a plasticity-based ice material model specifically designed for ship-iceberg impacts. This model employs an elastic-perfectly plastic material with a user-defined failure criterion that is based on hydrostatic pressure and effective plastic strain. It is pressure-dependent and strain-rate-independent. The researchers applied this material model in full-scale simulations, where a shuttle tanker's bow collides head-on with an iceberg modeled as a wall at two different penetration distances. To save computational time, the collision scenario was divided into external and internal mechanics. In these simulations, both the ice feature and the ship undergo plastic deformation, ensuring that energy dissipation is shared between the iceberg and the vessel. In Ref. [8], the authors also applied the model to examine a head-on impact with a ship's bow structure. They used two spherical-shaped iceberg features with different radii to simulate the collision, with the impact occurring at two different locations: once against a webframe and once midway between two webframes. Their findings indicated that the scenario where the iceberg collided midway between the webframes resulted in greater plate deformations compared to the collision directly on the webframe. Furthermore, Liu et al. [9] applied the model to study collisions on the side of a ship. The ship structure was based on that of an ice-strengthened Floating Production Storage and Offloading Unit (FPSO). They used various iceberg shapes, including sharp, blunt, and intermediate forms (circular or parabolic rotational symmetric). Different collision scenarios were simulated by varying the iceberg shapes and their impact locations, with each scenario representing a head-on collision on the gridstructured double hull. The location of the impact and the shape of the iceberg had significant influences on the results.

Building upon the work by Liu et al., Yu et al. [10] applied this model to study ice-structure interactions within the accidental limit state. They modeled and simulated ellipsoidal-shaped ice features with varying radii to pinpoint the critical geometry influencing impact on offshore structures. Both head-on and oblique impact scenarios were investigated.

Yu and Amdahl [11] utilized the ice material model developed by Liu et al. [7] in their numerical solver to simulate the coupled interactions of glacial ice impacts, taking into account the effects of hydrodynamic-ice-structure interaction. They examined several impact scenarios involving both a sharp and blunt ellipsoidal ice feature striking a structure at different angles. Their findings indicated that structures are more vulnerable to combined indentation and sliding loads compared to rectilinear indentation.

Similarly, Gagnon did full-scale ship-ice impact simulations. Gagnon [4] developed a crushable foam ice material model, which was later applied by Gagnon and Wang [12] in simulations involving a tanker being impacted by a bergy bit. The tanker's grillage was not ice-strengthened, and the impact occurred at the bow shoulder in a glancing manner. The study accounted for hydrodynamic effects using the arbitrary Lagrangian-Eulerian formulation in LS-DYNA.

Despite these studies, there is still a gap in understanding how different impacting ice shapes, impact locations on the ship, and varying impact angles together affect a collision between an ice floe and a ship hull that is not reinforced for ice. Our study addresses this gap by analyzing all these factors together over 18 simulations. For simulating ship-ice impacts, the Mohr-Coulomb nodal split (MCNS) model is used as the ice material model, developed by Herrnring [13]. The MCNS model combines the Mohr-Coulomb material which has higher compressive than tensile strength, with a nodal split approach that splits elements as soon as a critical plastic strain is reached. The model maintains mass conservation because no elements are eroded, except when the melting pressure occurs, defined as 110 MPa. This material model is developed for brittle ice behavior and is capable of showing crushing and spalling

behavior. It was validated by Herrnring [13] against both small- and large-scale laboratory experiments. Simulations by Müller et al. [14] using the MCNS model showed good agreement with experimental data. The ice strength of the MCNS model used in this study is similar to that of glacial ice.

The ice shapes used in the simulations are highly idealized, based on small-scale experiments. These experiments conducted by Müller et al. [14–16] investigated multiple ice shapes in drop-tower tests against both rigid and deformable plates. Among the shapes tested, the truncated cone and dome-shaped ice specimens caused the most significant plastic damage (deformation) to the deformable plates during impact, indicating that they are the most damaging shapes for head-on impacts with deformable plates. With rigid plates, ice shapes that were flat and parallel to the impacting structure resulted in the highest loads. The cone-shaped specimens demonstrated a high degree of energy dissipation when impacting a rigid plate. Due to the distinctly different behaviors exhibited by these shapes, they were selected to represent the base shapes in this study: round, flat-parallel, and sharp.

To better contextualize our findings, we consider both small-scale experiments and full-scale measurements to compare with our simulation results.

There is limited data available on full-scale ship-ice interactions with detailed local ice load measurements. However, one notable study was conducted by Ritch et al. [17] involving the CCGS Terry Fox, a Canadian Coast Guard heavy icebreaker. During this test program, the ship experienced 178 impacts with bergy bits weighing between 20 and 22,000 tonnes, at ship speeds ranging from 0.2 to 6.5 m/s. The bow of the ship was instrumented with 120 strain gauges, and 60% of the impacts occurred in the instrumented area. Measurements recorded pressures of up to 11.3 MPa on a contact area of 0.12 m² and forces reaching 5 MN. This, together with pressure-area curves derived from trials with Oden and the United States Coast Guard Cutter (USCGC) Polar Sea, as reported in Ref. [18], will be used to assess the extent to which the simulation results of our study correspond with real full-scale ship-ice impact loads. These data encompass impacts involving various types of ice, including first-year, multiyear, and glacial ice. In our material model, the ice is calibrated with a strength similar to glacial ice, based on laboratory frozen freshwater ice properties.

Through this comprehensive examination, the study aims to enhance our understanding of the critical parameters influencing ice impacts on non-ice-strengthened ship hulls, ultimately providing guidelines for utilizing FEM analyses with the MCNS model in full-scale ship-ice collision simulations.

2 Numerical Simulation Setup

For the full-scale simulations conducted, the explicit dynamic FEM solver LS-DYNA version 13.1 was used. The focus was on a non-ice-strengthened vessel, and the FEM model of this ship (shown in Fig. 1) was provided prior to this study, the modeling process itself falling outside the scope of this investigation. The simulation focused specifically on the starboard bow shoulder of the vessel, as this area is one of the most likely points of impact with ice floes. The zone where the ice impacts is modeled with shell elements of 20 mm edge length. The shell elements use the Belytschko-Tsay formulation, and five integration points through thickness with a shear factor of 0.8333 are used. The bulb flats in this region have shell elements for the web and beam elements for the bulb. Stiffener penetrations in the web frames, as well as lugs, are also taken into account. In the region away from the impact zone, a coarse mesh of shell elements with an edge length of 100 mm is used, where all stiffeners are modeled as beams in order to reduce calculation time. In between, a gradual transition is made. The material being used is an elastic-plastic type with the properties of S275 steel. More details can be found in Ref. [19]. The remainder of the ship (mass and inertia), which

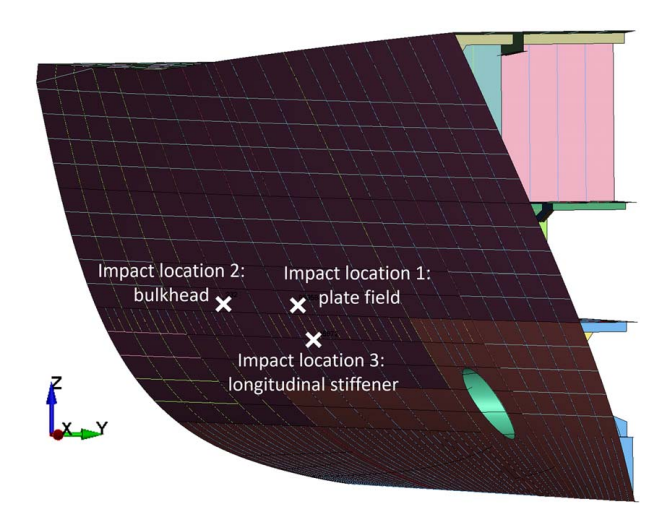


Fig. 1 Impact locations on the ships hull at the front starboard shoulder

was not explicitly modeled, was taken into account using the PART_INERTIA card in LS-DYNA. This involved incorporating the remaining mass and inertia with the appropriate center of gravity and coordinate system. Boundary conditions were applied at the ship's centerline to constrain translational movement in the z-direction (pointing downward) and rotational movement around the x-axis (pointing forward) and the y-axis (pointing portside). The vessel's motion was initiated using the INITIAL_VELOCITY card, applying an initial velocity of 2 m/s (3.9 kn) to the ship. The centerline of the ship was oriented with the global x-direction (0 deg) and the ship moved in various translational directions (0 deg, 30 deg, 60 deg, and 90 deg), as shown in Fig. 2. This movement resembles a drifting motion and is intended to cover the range of impact angles experienced during maneuvering, including glancing, head-on, and intermediate impacts.

The ice bodies were only partially modeled, with emphasis on the contact shape involved in the impact, as shown in Fig. 3. These shapes are consistent with those used in laboratory experiments conducted by Müller et al. [14–16] and represented three primary categories: round, flat-parallel, and sharp. The round shape is characterized by a smooth and continuous surface and was modeled as a dome-tipped cylinder with a diameter of 800 mm (Fig. 3(a)) for simulations. The flat-parallel shape features a level, even surface that is parallel to the structure impacted. For simulation, a truncated cone-tipped cylinder with a cone angle of 120 deg, a lower diameter of 800 mm, and an upper diameter of 400 mm was used (Fig. 3(b)). The sharp category exemplifies forms with pointed tips, such as pyramids or spikes. In the simulation, a cone tipped cylinder with a 120 deg angle was used (Fig. 3(c)). For simplicity, in the following, we will refer to the shapes as the dome, truncated cone, and cone, without noting the tipped cylinder. The hydrodynamic effect was disregarded, with the exception of the added mass of the ice floe in the main direction of movement during the impact (the y-direction) being added to the mass in PART_INERTIA. The

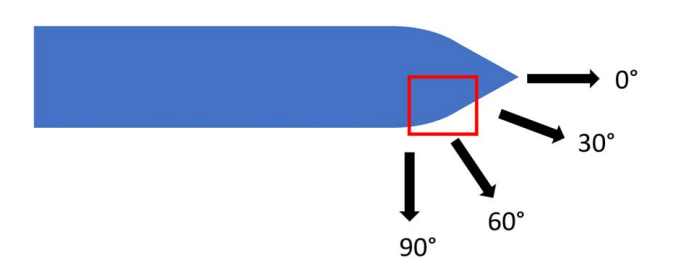


Fig. 2 Angles of translational ship movement. The modeled part of the ship is marked with a box

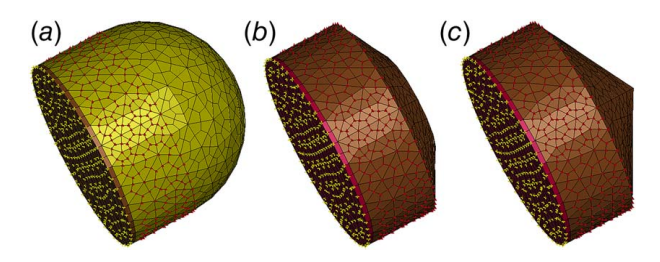


Fig. 3 Ice impact shapes with constrained nodes marked. Nodes marked with a triangle: relative movement between the nodes is constrained; nodes marked with a cross: a boundary condition is applied so that movement in z-direction is constrained. (a) Dome (round), (b) truncated cone (flat-parallel), and (c) cone (sharp).

added mass was calculated using the large amplitude ship motions program (LAMP). The LAMP run was setup as an infinite-frequency domain problem. Boundary conditions were applied to the rigid part of the ice body, indicated by small crosses at the nodes in Fig. 3, to prevent movement in the *z*-direction. Additionally, the circumference nodes of the cylindrical part, marked with triangles in Fig. 3, were constrained to prevent relative movement between them.

The modeled portions of the shapes were oriented orthogonally to the hull shape. The shapes were positioned as close as possible to the impact point, minimizing the distance of no contact. The modeling of the ice geometries, the ice material model, and the contact definitions were chosen according to the Mohr-Coulomb nodal split model developed by Herrnring [13]. The geometries were initially created using Ansys ADPL Mechanical, with a tetrahedral mesh and a size of 0.1 m. Subsequently, the shapes were imported into LS-PrePost, where the elements were split into hexahedral elements with a size of 0.05 m, as recommended by Herrnring and Ehlers [5]. In LS-Dyna, the 173-MOHR_COULOMB material card was used as an ice material in conjunction with a node-splitting approach, wherein the nodes are split once a critical plastic strain of 0.002 is reached. The uniaxial compression failure of the ice material is defined as 5.23 MPa and the elastic shear modulus as $3.5 \times 10^9 \,\mathrm{Pa}$. The unmodeled portion of the ice is represented using the PART_INERTIA card, accounting for the mass of a 25 \times 25 m ice floe with a thickness of 1 m, along with its inertia, center of gravity, and coordinate system. The ice was constrained to prevent movement in the z-direction and was stationary until impact.

The contact between individual ice elements was defined using the AUTOMATIC_SINGLE_SURFACE and the ice-hull contact

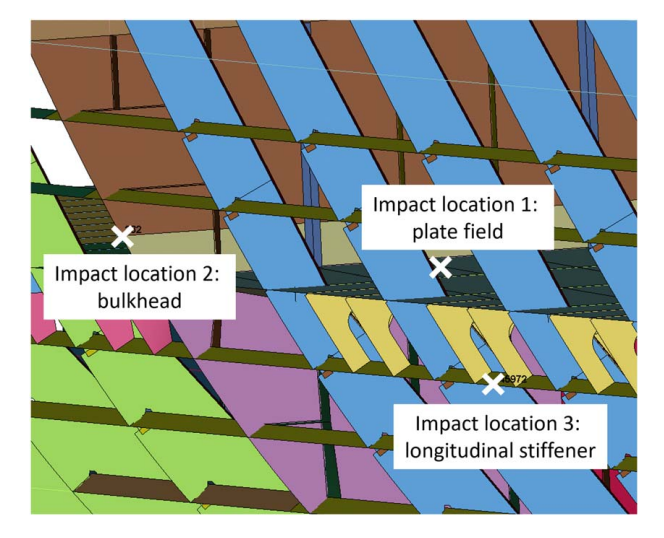


Fig. 4 Impact locations at the ships structure without shell plating

Table 1 Simulation matrix

Impact velocity	2 m/s
Impact location	1: Plate field
	2: Bulkhead
	3: Longitudinal stiffener
Impact angle	0 deg
	30 deg (only at impact location 1)
	60 deg (only at impact location 1)
	90 deg (only at impact location 1)
Impact shape	1: dome (round)
	2: Truncated cone (flat-parallel)
	3: Cone (sharp)

was realized with an AUTOMATIC_SURFACE_TO_SURFACE card. For more details on the MCNS model and the contact definition, please refer to Refs. [5] and [13].

Three distinct impact locations were tested and are shown in Figs. 1 and 4: the plate field (location 1), bulkhead (location 2), and longitudinal stiffener (location 3). All three impact locations are within the area where ice contact is possible. These locations were chosen to represent a wide range of hull stiffness and deformation behavior during a glancing impact. The plate field has the lowest stiffness. The bulkhead impact location has a stiff structural member oriented perpendicular to the impact direction. The third impact location is at a longitudinal stiffener that runs horizontally in the same direction as the impact and is supported by brackets. The main focus is on the glancing impact (0 deg), as it is the most likely scenario. Therefore, this impact is studied at all three locations. Other impact angles are only studied at the plate field. This approach allows for a comparison with experimental data, where a head-on impact on a nonstiffened plate was tested. The general test matrix, including all simulations, is outlined in Table 1. The shell plating at all three impact locations is 9 mm. The bulkhead has a plate thickness of 6 mm from impact location 2 and above (brown plating in Fig. 4) and below 10 mm (gray plating in Fig. 4). The longitudinal stiffener at impact location 3 is of type HP140 \times 7. The frame spacing is 1800 mm, and the stiffener spacing is close to 600 mm. The dimensions of the frames are $T350 \times 8/120 \times 12$.

3 Results and Analysis

This section presents an overview of the simulation results, divided into three parts that analyze the influence of impact direction, impact shape, and impact location. The analysis examines LS-DYNA outputs from the matsum, glstat, reforc, d3plot, and intfor files. The key physical components examined include contact force, internal energy, relative resultant displacement, contact area, effective plastic strain, and pressure. The ascii and intfor output data are sampled at intervals of 0.001 s, whereas the d3plot is sampled at intervals of 0.02 s.

3.1 Analysis of the Influence of Impact Direction. Initially, the influence of the direction of impact is analyzed. Therefore, the results of the simulations of impact location 1 (plate field) for all four angles of impact are analyzed.

Figure 7 shows typical force-time histories of an impact simulation from each direction for the truncated cone ice geometry interacting with the plate field. The impact force initially increases as the bodies come into contact, reaching a maximum before decreasing back to zero as the ice is pushed away from the ship, resulting in no further contact between the bodies. The maximum force increases as the impact angle goes up to 60 deg. From 60 deg to 90 deg, the maximum force remains unchanged. As the angle increases from the 0 deg glancing impact to a 90 deg perpendicular impact, the magnitude of the impact increases. The maximum force ranges from 0.5 to 3 MN. For a 0 deg glancing impact, the force is







Fig. 5 This simulation shows the tip of a truncated cone-shaped ice floe hitting the plate field (location 1) at an impact angle of 60 deg. There are three states shown: on the left, before the ice touches the plate; in the middle, during contact; and on the right, at the point of maximum penetration.

about 17% of that for a 60 deg or 90 deg perpendicular impact. This trend is similar for the other two shapes. The interaction between the ice and the ship is shown in Fig. 5 for three stages: before contact, during impact, and at maximum penetration. The plate undergoes severe deformation, while the ice experiences only moderate deformation. The deformation of the ice floe tip is shown in Fig. 6 at a hitting angle of 60 deg. As the ice is pushed further into the ship's hull, the edge of the truncated cone becomes more rounded. The ice elements are confined between the hull and the constrained part of the ice body, and only a few elements separate from the ice body (Fig. 6).

A similar pattern is observed in the internal energy results, as depicted in Fig. 8. The same case as above is shown here: a truncated cone impacting the plate field across all four angles of impact direction. The figure shows the internal energy, separated for both the ship and the ice. In all scenarios, the ship's internal energy is greater than that of the ice, decreasing with the impact angle from 90 deg to 0 deg. The ratio of the ship's to the ice's internal energy ranges from 6 to 12, meaning that the ship deforms more during the collision than the ice. High ice strength and low hull stiffness contribute to overall deformations. The time history of the ship's internal energy consistently exhibits a minor peak, which recovers postimpact due to the elastic deformation of the ship's hull.

Load–deformation curves illustrate the responses of both the ship and ice during an impact. The strain energy is represented by the area under these curves. The ship's structure and the ice possess differing relative stiffness, resulting in deformation and energy dissipation primarily occurring in the weaker material. Figure 9 presents the load-deformation curves for the impact of a truncated cone at impact location 1 (the plate field). For the structural side, the plate node that experienced the highest plastic deformation during impact was used to measure the deformation. On the ice side, a node located at the edge of the truncated cone-shaped ice apex (shown in Fig. 6 with a dotted line) was used, as this is where the largest deformations occur. Since the material model allows for nodal splitting, we chose a node that remained attached to the ice body until the maximum force was reached. Due to the confinement of the ice tip between the ship hull and the constrained part of the ice body, a representative node was found in all impact cases involving the truncated cone. Displacements at these nodes were measured



Fig. 6 Deformation of the truncated cone ice body during the collision with the ship at a 60 deg angle. Left: before contact; middle: during contact; and right: max deformation of ice during impact. The dotted circle marks the edge of the truncated cone, where the ice deforms the most. A node along this line was selected for the upcoming force-deformation curves.

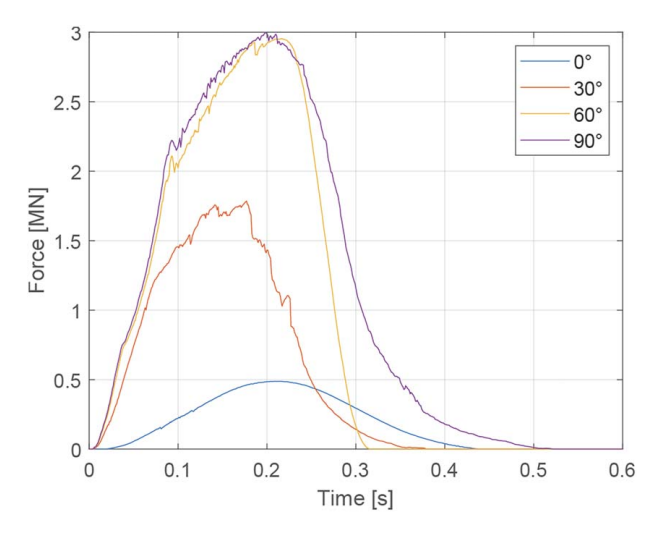


Fig. 7 Force-time histories of the impact of a truncated cone hitting the ship at impact location 1 (plate field)

relative to a fixed point on the ship or ice, ensuring that the reference point did not deform. In this scenario, the ice behaves in a very rigid manner compared to the ship's structure, which undergoes significant deformation and dissipates most of the energy from the impact. When the impact direction changes, the stiffness of the hull—indicated by the slope of the force—deformation curves—varies within a small range but remains mostly similar. However, both the deformation and the force on the ship's side increase as the impact angle grows. Notably, the results for impact angles of 60 deg and 90 deg are very similar. For ice, both the force and deformation increase as the impact angle increases. However, at a 30 deg impact angle, the deformation is larger compared to other angles. The maximum deformations for impact angles of 60 deg and 90 deg are quite similar.

3.2 Analysis of the Influence of Impact Shape. The trend observed above indicates that the internal energy of the ship is higher than that of the ice; however, this observation is not consistent across all ice impact shapes. For the dome-shaped ice, higher impact angles (60 deg and 90 deg) result in greater internal energy for the ice compared to the ship for a brief period during the impact, as shown in Fig. 10 for the perpendicular impact. At impact angles of 0 deg and 30 deg, the dome-shaped ice leads to

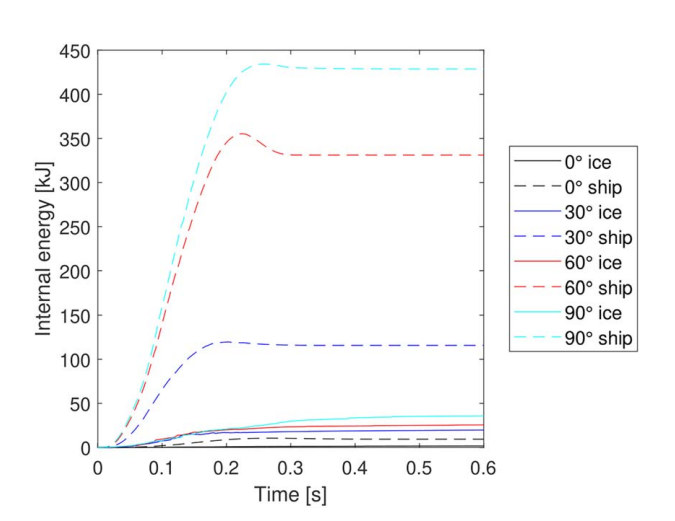


Fig. 8 Internal energy of truncated cone impact at plate field in different impact directions

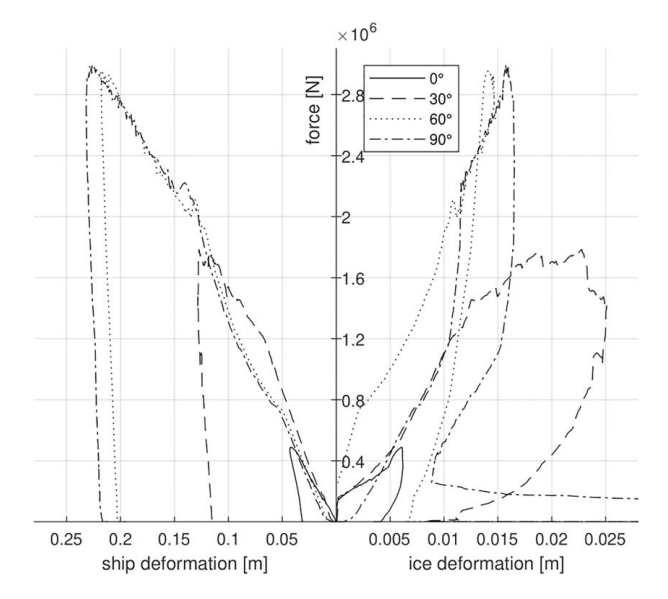


Fig. 9 Load-deformation curves for the impact of the truncated cone ice shape at impact location 1 (plate field) for different impact angles

higher ship's internal energy than the other two ice impact shapes. For 60 deg and 90 deg impact angles, the truncated cone shape exhibits the highest values of the ship's internal energy, followed by the cone and then the dome.

The truncated cone shape generally induces the highest forces, followed by the cone and the dome in most cases, as shown in Fig. 11. An exception is observed in the case of a glancing impact (0 deg) at impact location 1 (plate field), where the dome exhibits higher forces than the cone, as depicted in Fig. 12. The peaks are offset from one another because the impacts start at slightly different times due to the different shapes. Additionally, the time it takes for the ice to be pushed away by the ship and the contact to end also varies. As shown in Fig. 12, the impact with the truncated cone lasts only about half as long as impacts with the other two shapes. In contrast, the internal energy of the ship is lower for impacts involving the truncated cone and the cone and higher for impacts with the dome, as illustrated in Fig. 13.

When examining the maximum plastic plate deformation in the plate field postimpact, shown in Fig. 14, the trend is similar to the force: the greatest deformations occur due to the impact with

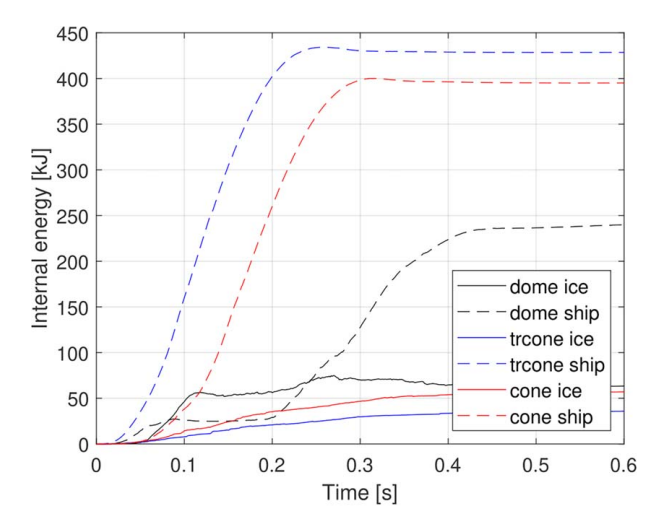


Fig. 10 Internal energy for the perpendicular impact (90 deg) at impact location 1 (plate field) for all three ice impact shapes

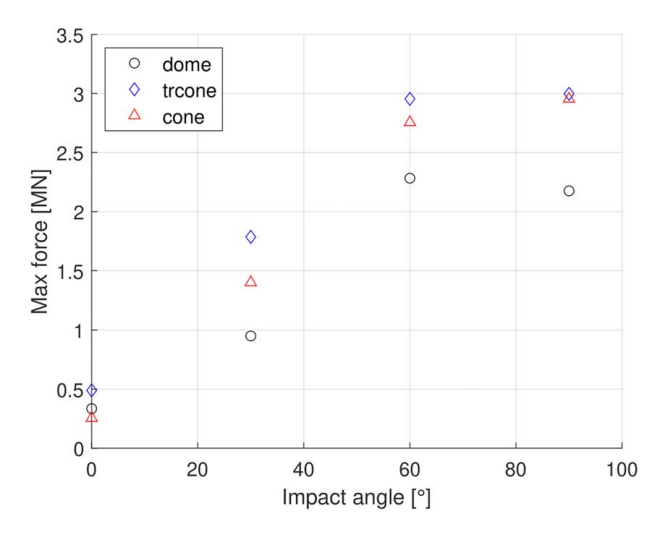


Fig. 11 Maximum forces over impact angle for impact location 1 for dome, cone, and truncated cone ice impact shapes

the truncated cone ice floe, followed by the cone and the dome. However, for a 0 deg glancing impact, the dome causes the highest deformation, followed by the cone and the truncated cone. Both the max forces (Fig. 11) and max hull deformations (Fig. 14) display a sinusoidal trend when considering the waterline angle of approximately 10 deg.

3.3 Comparison of Different Impact Locations. Significant differences are observed across various impact locations. As shown in Fig. 15, the maximum forces for all three impact locations and impact shapes in a glancing impact (0 deg impact angle) were analyzed. The truncated cone and dome-shaped specimens exhibit the highest force when impacting the bulkhead, IL2, while the cone shape yields similar results regardless of the impact location. A similar trend is observed in the internal energy, as illustrated in Fig. 16. When examining the maximum deformations of the plate for all glancing impacts (Fig. 17), we find that the greatest deformations occur when the dome hits the plate field (IL1), followed by the cone at IL1. Generally, the displacements at impact location 1 are larger than those at locations 2 and 3. This difference can be attributed to the local reinforcement provided by the longitudinal stiffener and the bulkhead preventing local deformations. The elastic-plastic strain, shown in Fig. 23, is highest at impact locations 1 and 2.

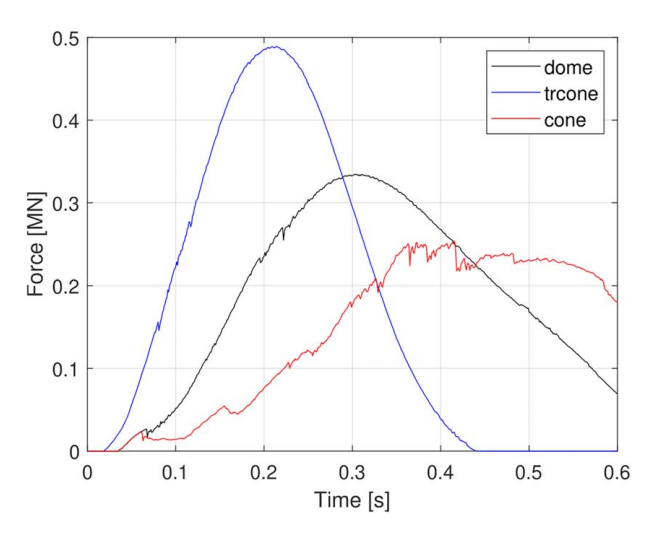


Fig. 12 Glancing impact (0 deg) at impact location 1 (plate field)

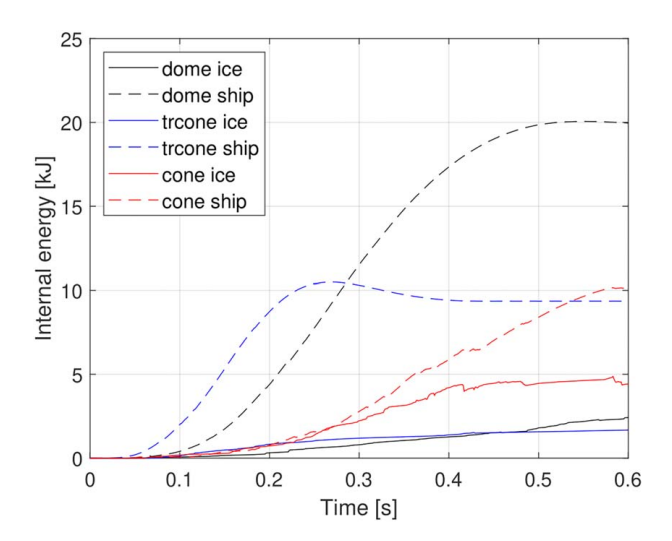


Fig. 13 Internal energy for the glancing impact (0 deg) at impact location 1 (plate field) for all three ice impact shapes

An example of a collision is shown in Fig. 18. The dome-shaped ice floe tip along with the ship at the bulkhead impact location is illustrated. The box highlights the area shown in detail in the following figures (Fig. 19). When the ice body strikes the bulkhead, it is crushed, and pieces break off from the main ice body. The ice is then pushed away from the ship, causing little impact on the structure behind the bulkhead.

Using the load–deformation curve for analysis, Fig. 20 illustrates the impact of the truncated cone-shaped ice body during a glancing impact (impact angle equals 0 deg) at all three investigated impact locations. Within the ship structure, nodes were selected to investigate points of maximum deformation during impact. In the case of the bulkhead, this point is located in the plate field in front of the bulkhead, whereas for the longitudinal stiffener, it is in the plate field above the stiffener. For the ice, a node at the edge of the truncated cone shape was selected because this is where the deformations are highest. When the impact occurs on the plate field, the ice behaves much more rigidly compared to the ship's structure, causing the structure to experience more significant deformation. A similar situation occurs when the impact is on the longitudinal stiffener. Here, the force remains constant for a period, while the deformation increases. This happens because the ice continues to move toward the specific node on the hull being examined. For

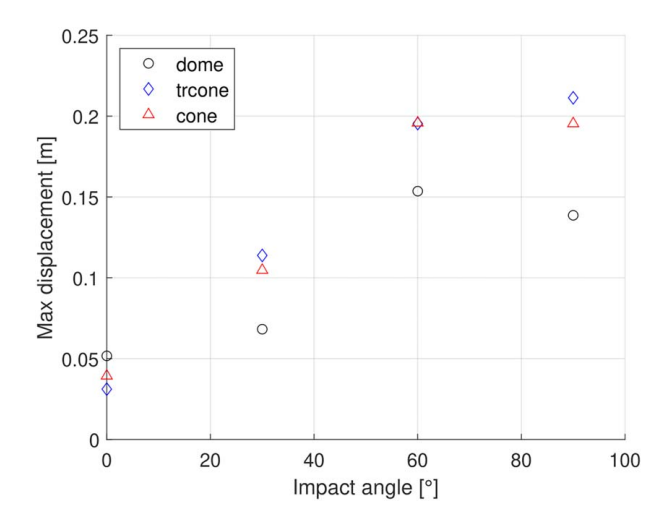


Fig. 14 Maximum plastic plate displacements over impact angle for impact location 1 for dome, cone, and truncated cone ice impact shapes

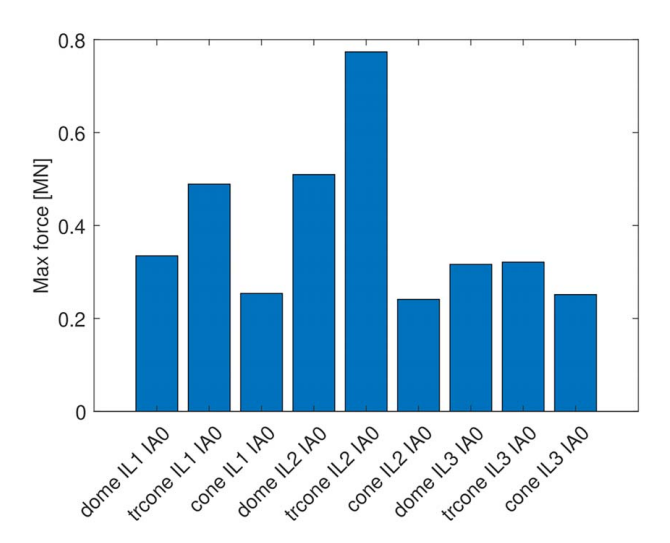


Fig. 15 Maximum forces for the 0 deg glancing impact at all three impact locations and shapes

impacts at the bulkhead, the deformations of the ice and the ship's structure are comparable. Initially, the structure deforms more while the ice deforms less, but as the load increases, the structure's deformation decreases, and the ice begins to deform more. This behavior is due to the sliding nature of impact. At first, the ship structure behaves similar to the impact on the plate field because the interaction starts in front of the bulkhead in the plate field. As the ice moves toward the bulkhead, where the structure is stiffer, the ice deforms more. The deformations of the ice following the peak load might be attributed to node splitting; otherwise, there would be no further increase in deformation. All three ship deformation curves demonstrate elastic recovery.

4 Discussion

The trends observed in the numerical analysis are compared with experimental results and full-scale measurements. Additionally, the worst-case scenario is examined, along with a discussion of limitations and recommendations.

4.1 Comparison With Experimental Data. Müller et al. [14,15] conducted small-scale experiments to investigate the

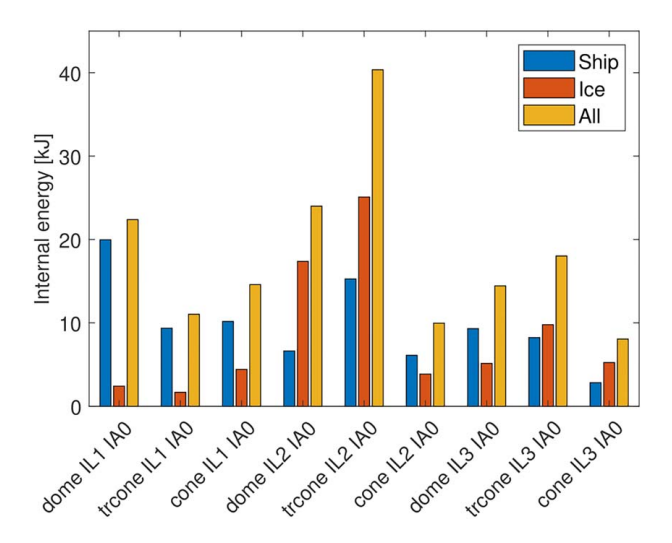


Fig. 16 Internal energy for the 0 deg glancing impact at all three impact locations and shapes

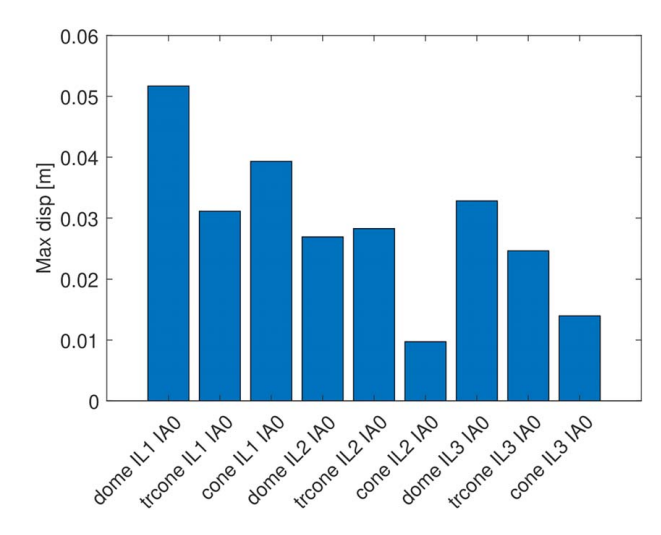


Fig. 17 Maximum plastic plate displacements for the 0 deg glancing impact at all three ILs and shapes

effect of ice shape on ice-structure interaction. These drop-tower experiments, using the same ice shapes as in our study, were head-on impacts that are comparable to our 90 deg impact simulations. Ice samples with a diameter of 200 mm (compared to 800 mm in our simulations) were dropped onto a round steel plate that is 3 mm thick and 400 mm in diameter, at a speed of 2 m/s. The ratio of the plate's diameter to its thickness is about 133. In the simulations, the plate measures between stiffening 1800 mm in width, 600 mm in height, and has a thickness of 9 mm. This results in a width-to-thickness ratio of 200 and a height-to-thickness ratio of 67, which averages to approximately 133 as well. Since the ratios are of the same order of magnitude, the stiffness of the experimental plate and the simulated plate can be considered comparable. The experiments measured impact force, hammer displacement, and postimpact plastic deformation of the steel plate. For additional details, please refer to the original studies. The experiments and simulations share several similarities: the ice shape, impact velocity, the fact that both the ice and the structure undergo plastic deformation, and the nearly head-on nature of the impact. However, key differences include the ice specimens' diameters (200 mm in experiments versus 800 mm in simulations) and varying impact

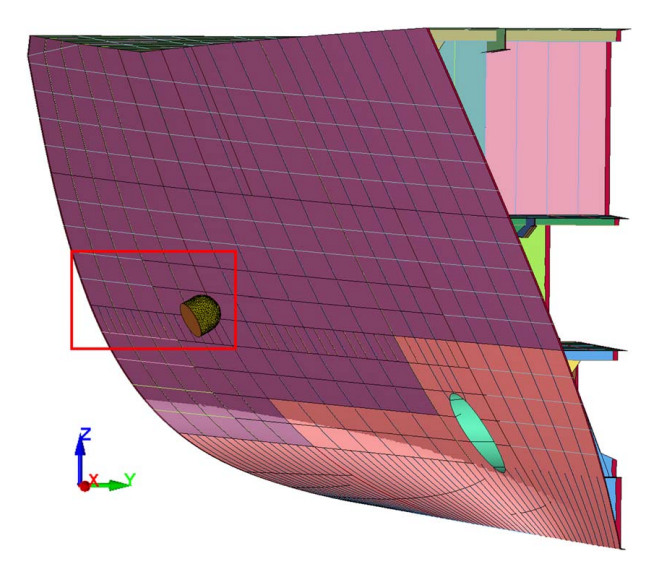


Fig. 18 Impact scenario in which the dome-shaped ice body strikes the bulkhead (IL 2). The rectangle highlights the area shown in detail in the following figures.

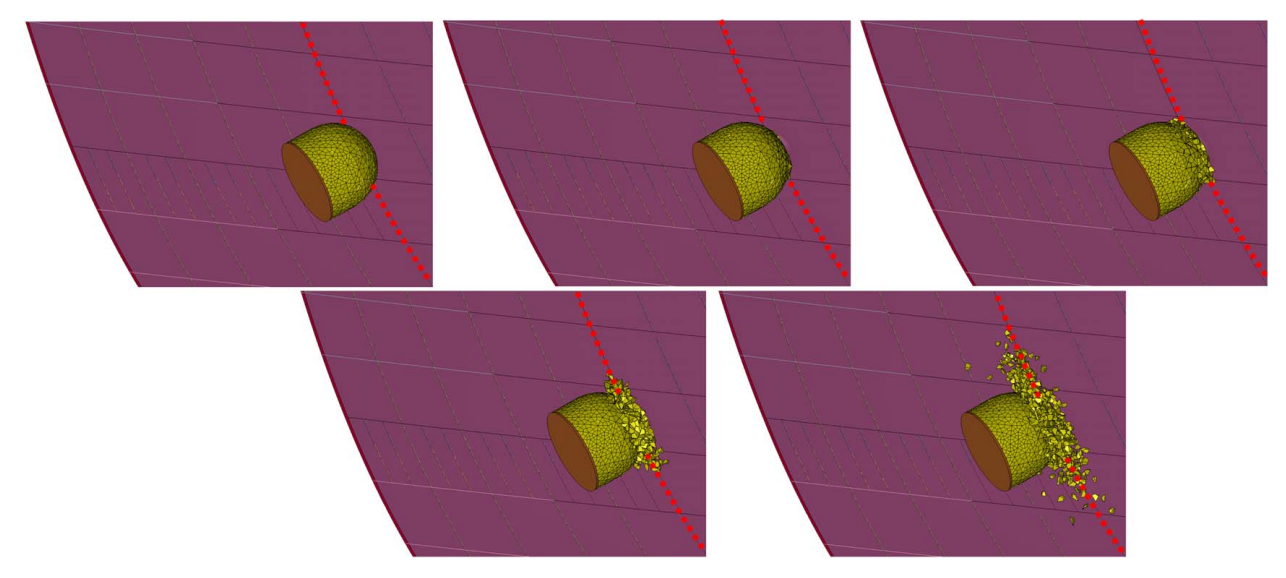


Fig. 19 Snapshots of the simulation showing the dome-shaped ice body impacting the bulkhead, indicated by a dotted line

energies due to different moving masses. Additionally, the constraints differ: in the experiments, the plate is fixed in all degrees-of-freedom, and the ice moves only in the vertical falling direction, whereas in the simulations, both the ship and ice are constrained only in the z translational direction. Furthermore, the ship's rotation around x- and y-axis is constrained. Consequently, results are compared only qualitatively to assess whether the trend among different ice shapes in the simulations reflects those observed in the experiments. When plotting experimental and numerical data on the same graph, we have to adjust both sets for a qualitative comparison. We assume that the relative load between different shapes does not change significantly when the size of the ice sample changes. First, we set the value of the truncated cone from the experimental data to 1. Then, we scale the values of the other shapes relative to this. Additionally, the numerical data are normalized using the force value of the truncated cone from the experiments. This approach allows for a qualitative comparison between the experimental and numerical results.

Fig. 20 Force over the deformation of ice and ship at selected nodes for the glancing (0 deg) impact of the truncated coneshaped ice body impacting all three locations

In the drop-tower experiments, the truncated cone exhibited the highest force, followed by the dome and the cone (Fig. 21). The plastic plate deformation was greatest for both the truncated cone and the dome, with the cone demonstrating significantly smaller deformations. In the current study, the numerical analysis indicates that the truncated cone-shaped ice floe experiences the highest forces (Fig. 21) and deformations which is in line with the experiments. However, unlike the experimental results, the cone showed higher values for both the maximum force and deformation than the dome. The exact reason for the different behavior of the dome-shaped specimen in the simulations remains unclear. One possible explanation is the variation in the failure mode of the ice body. In the study by Müller et al. [14], the experiments were used to validate the MCNS model. The comparison revealed that

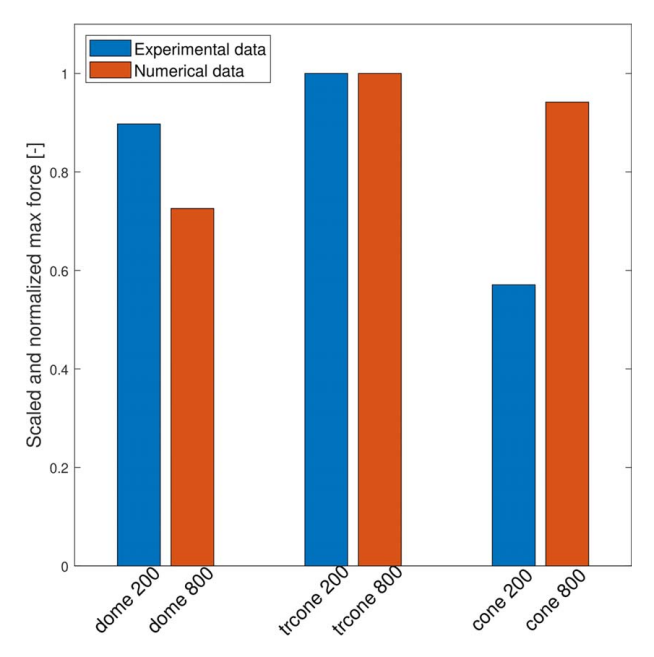


Fig. 21 Experimental versus numerical data of the max force for qualitative comparison. The values of the truncated cone from both the experiment and the simulation are normalized by setting the value to one, and then all other values are scaled accordingly.

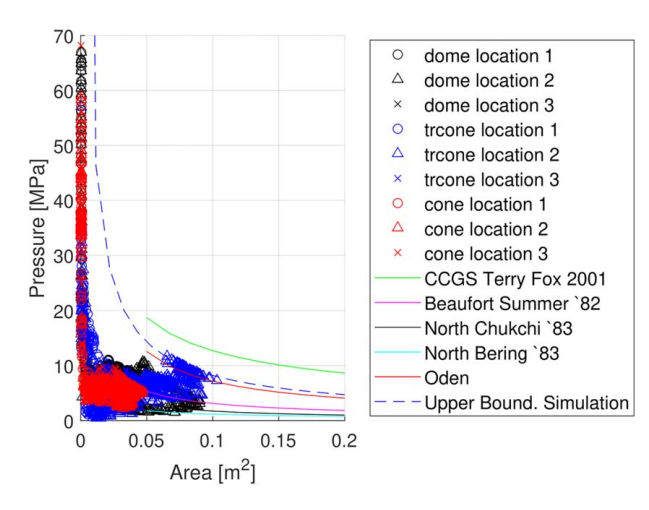


Fig. 22 Pressure–area data for impact location 1 (plate field) for the glancing impact together with pressure–area curves of fullscale measurements

in the simulations, the dome exhibited lower forces and a broader peak load due to continuous crushing, which was the dominant failure mode. In contrast, the experiments showed axial cracks, resulting in a much narrower load peak. This difference in failure mode affects the contact area, which in turn influences the pressure and deformation caused by the ice on the impacted structure.

4.2 Comparison With Literature Data. The results of current numerical simulations have been compared with full-scale load measurements. Specifically, data from trials conducted with the CCGS Terry Fox in 2001 by Ritch et al. [17] are utilized, along-side several other trial datasets collected in Ref. [18]. The pressure—area curves fitted to these trial datasets are compared against the pressure—area scatter derived from the numerical analysis involving the glancing impact at all three impact locations with all three impact shapes, as shown in Fig. 22. An upper boundary curve is fitted to the simulation data, represented by the dashed line. The curves from full-scale trials are plotted only for areas of 0.05 m²

Table 2 Pressure-area coefficients and ice type

Data set	C_P	D_P	Ice type
CCGS Terry Fox 2001	3.5	-0.56	Bergy bits
USCGC Polar Sea	0.53	-0.77	Multiyear ice of mainly 3 m
Beaufort Summer 82			thickness
USCGC Polar Sea	0.38	-0.79	Medium and thick first-year ice of
North Chukchi 83			0.9–1.8 m thickness
USCGC Polar Sea	0.28	-0.62	Thin and medium first-year ice
North Bering 83			with 0.15-1.2 m thickness
Oden	1.11	-0.81	Multiyear ice
Upper Bound.	1.3	-0.80	Laboratory grown granular fresh
Simulation			water ice with 0.8 m thickness

and larger, as this threshold represents the lower limit and is even already below the measured areas during the trials.

When examining the numerical data, the pressure values range from 2 to 70 MPa for contact areas up to $0.10\,\mathrm{m}^2$. The highest pressures occur at all three locations on very small contact areas using the dome-shaped and cone-shaped specimens. The cone-shaped specimen consistently shows smaller contact areas with values up to $0.05\,\mathrm{m}^2$ compared to the other two ice shapes. The truncated cone-shaped and dome-shaped specimens exhibit larger contact areas up to $0.10\,\mathrm{m}^2$, where pressures predominantly remain below $12\,\mathrm{MPa}$.

When comparing the simulation data with the full-scale measurements, it appears that the simulation results fall within the range of measurements. The CCGS Terry Fox and Oden are at the upper end, with the upper boundary curve of the simulation being close to the Oden curve, while the USCGC lies at the lower end. This appears reasonable, as the trial data from the CCGS Terry Fox and Oden represent bergy bits and multiyear ice, respectively, which, despite having much larger ice thicknesses, are similar in strength to the ice used in the simulation. Nevertheless, the significantly lower contact areas resulting from the simulations, compared to full-scale measurements, make it difficult to put the results into perspective. Furthermore, the ships used in the trials are all icebreakers and, therefore, heavily ice-strengthened. This means that even though we assume the ice conditions, in terms of ice strength, are comparable, the response of the hull differs from that of our study's sample

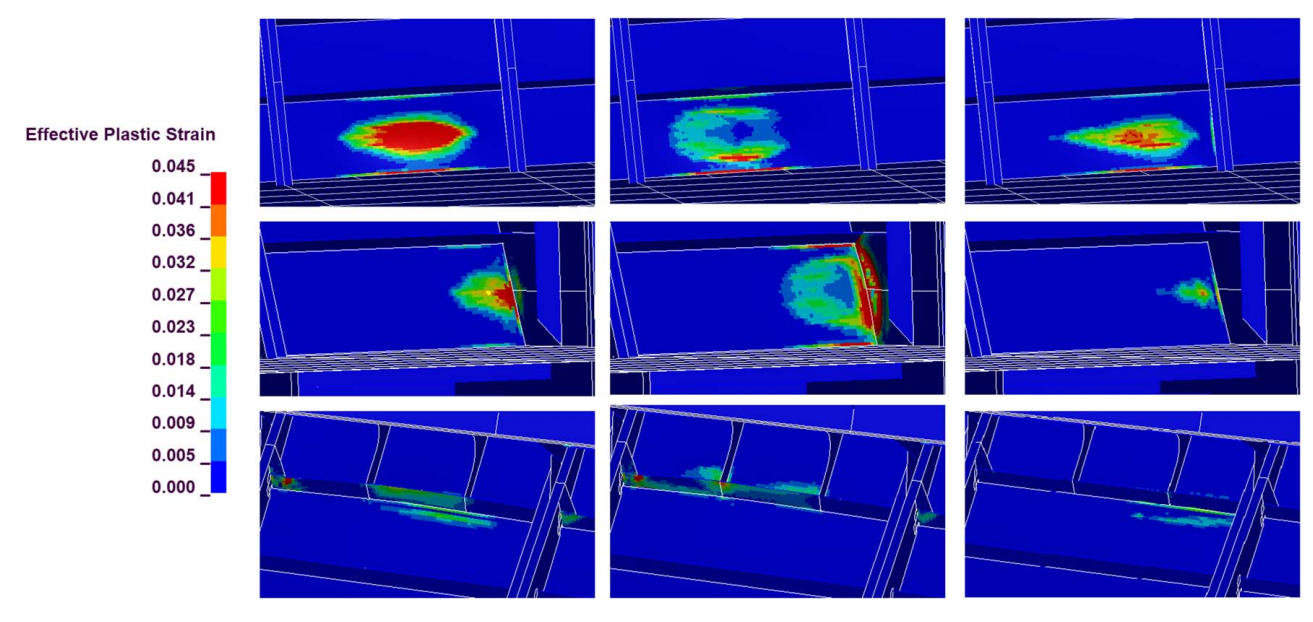


Fig. 23 Effective plastic strain at impact locations is shown in three lines: top for plate field, middle for bulkhead, and bottom for longitudinal stiffener. Each row displays results for ice shapes from left to right: dome, truncated cone, and cone. The legend on the left applies to all figures.

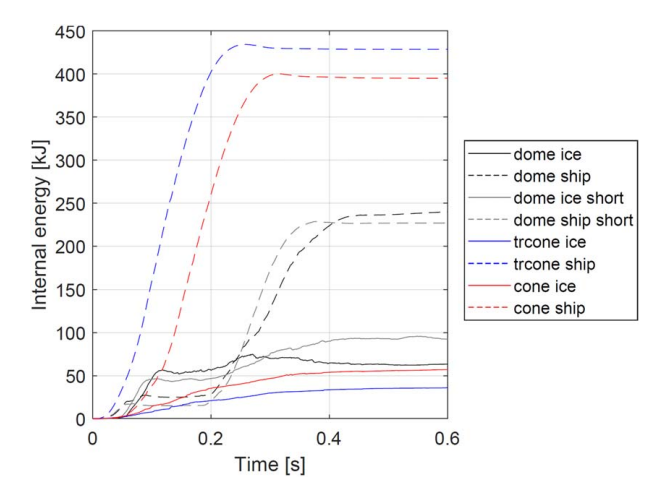


Fig. 24 Internal energy for a 90 deg impact at location 1 on the plate field. For the dome shape, two sets of curves are presented: one from the standard simulation and another from the simulation with adjusted volume, labeled as 'short.'

vessel. Ice-strengthened ships are significantly stiffer and deform less, affecting both the pressure exerted and the contact area during impact. The function used to describe the trial curves is presented below with the input data and ice type provided in Table 2.

$$P = C_P A^{D_P} \tag{1}$$

4.3 Worst Case Scenario, Limitations, and Recommendations. The worst-case scenario among those studied is the impact that causes the greatest force, the largest deformation, or the highest plastic strain. The worst-case scenario for the glancing (0 deg) impact depends on our focus: either the truncated cone or the dome impacting the bulkhead or the plate field. The highest forces are observed when the truncated cone strikes the bulkhead, which is a very rigid structure. This is in line with findings from Riska et al. [20]. They found that the frames in a framed structure, being more rigid than the plates, carry more load. Meanwhile, the greatest plate deformation occurs when the dome-shaped ice impacts the plate field. Additionally, the largest plastic strain is recorded when either the dome or the truncated cone hits the bulkhead or the plate field. The cone-shaped ice feature does not produce high forces, but when it strikes the plate field, it causes quite large deformations and strain.

The primary limitations of these simulations include the absence of hydrodynamic and hydrostatic effects, as well as the lack of a failure criterion for the steel hull. Additionally, exact validation of these simulations is not feasible due to the unavailability of corresponding full-scale experimental data. In these simulations, the ice shapes have different volumes. However, when the volume of the dome-shaped ice is adjusted to match the smaller volumes of the cone and the truncated cone, the initial and adjusted results showed only slight variation. Figure 24 shows the internal energy, which was initially expected to depend greatly on the volume of the ice. The plot shows that the energy values are slightly different, but these differences do not significantly affect the overall comparison.

These simulations are computationally intensive; simulating a 0.6 s impact requiring approximately 20 h of processing time on 16 CPUs with a 2.3 GHz processor.

When investigating the worst-case scenario in full-scale ship-ice glancing (0 deg) impact simulations using the MCNS model with FEM, a flat ice contact shape oriented parallel to the hull is recommended. These ice shapes result in the highest forces. Alternatively, a round shape can be used; although it results in lower loads, it is somewhat more realistic than a flat surface parallel to the ship's hull and leads to high plastic strains and deformations. Sharp

shapes are not recommended, as they do not yield conservative results in most cases. The performance of the MCNS model for different shapes during a glancing impact has not yet been tested against experimental data. So far, it has only been validated through experiments involving a head-on impact against a rigid plate, as reported in a study by Müller et al. [14]. In that study, the model showed strong performance with sharp shapes like cones and did well with flat shapes such as truncated cones. However, the results were not as precise for dome-shaped ice, especially concerning peak force and failure mode.

Areas of interest for investigations of dynamic ice impact on non-ice classed ship hull structure should include sliding loads affecting locations where local reinforcement of the shell plating generates a significant change in structural stiffness perpendicular to the direction of impact, such as at a bulkhead or transverse framing. Additionally, investigations should include regions with low structural stiffness such as in the plate field.

5 Conclusion

This study numerically examined ship-ice impact scenarios investigating the influence of impact angle, impact location, and ice shape on the resulting maximum force and structural deformation. The key findings are as follows:

- All three parameters (shape, location, and angle) significantly influence the impact force and structural deformation.
- The most vulnerable impact location varies depending on the impacting ice shape used. The highest forces in a glancing impact are observed at impact location two, the bulkhead.
- As the impact angle increases, both the force and plastic deformation of the ship's hull increase. For a glancing impact, the force drops to 17% of that experienced during a perpendicular impact.
- The force and internal energy are highly dependent on the shape of the impacting ice.
- Comparison with small-scale experimental data revealed that the different ice shapes, especially the dome-shaped ice, do not behave as expected. Based on qualitative comparison, the simulated force and plastic plate deformation are too low relative to other shapes.
- Comparison with full-scale measurements indicates that the pressure-area relationship observed in the simulations is reasonable. However, the contact areas in the simulations tend to fall at the lower end of the range found in the full-scale data, which makes it challenging to fully contextualize the results.

The simulation used the MCNS ice material model to investigate certain influence parameters in full-scale ship-ice collision scenarios using the explicit dynamic LS-DYNA solver. Hydrodynamics and hydrostatics were mostly neglected and specific boundary conditions were applied. Full-scale simulations of ship-ice interactions often face the challenge of lacking comprehensive validation data sets that encompass all ice and ship properties, leaving uncertainty about how accurately the simulations represent real scenarios. However, the simulations produced reasonable pressure-area values compared to the available ice impact data sets. The study also demonstrated that a material model for ice should be versatile enough to be applied to various ice shapes without requiring adjustments. This is crucial because the shape of the ice significantly influences the resulting loads on the structure. This study serves as a preliminary investigation for future numerical analyses, in which hydrostatic and hydrodynamic effects will be included. Additionally, future simulations should incorporate realistic ice apex shapes rather than idealized ones to enhance the accuracy and applicability of the results.

Acknowledgment

This work was supported by the US Office of Naval Research Global (ONRG) under the NICOP Grant N62909-22-1-2019. It is stated that the funder is not responsible for any of the content of this publication.

Conflict of Interest

There are no conflicts of interest.

Data Availability Statement

The datasets generated and supporting the findings of this article are obtainable from the corresponding author upon reasonable request.

References

- Popov, Y. N., Faddeev, O. V., Kheisin, D. E., and Yakovlev, A. A., 1969, "Strength of Ships Sailing in Ice," Technical Report No. FSTC-HT-23-96-68.
- [2] Daley, C., 1999, "Energy Based Ice Collision Forces," Proceedings of the 15th International Conference on Port and Ocean Engineering Under Arctic Conditions (POAC), Espoo, Finland, Aug. 23–27, Vol. 2, Citeseer, pp. 674–686.
- [3] Daley, C., and Kim, H., 2010, "Ice Collision Forces Considering Structural Deformation," International Conference on Offshore Mechanics and Arctic Engineering, Shanghai, China, June 6–11, Vol. 49125, pp. 817–825.
- [4] Gagnon, R. E., 2011, "A Numerical Model of Ice Crushing Using a Foam Analogue," Cold Reg. Sci. Technol., 65(3), pp. 335–350.
- [5] Herrnring, H., and Ehlers, S., 2022, "A Finite Element Model for Compressive Ice Loads Based on a Mohr-Coulomb Material and the Node Splitting Technique," ASME J. Offshore Mech. Arct. Eng., 144(2), p. 021601.
- [6] Mokhtari, M., Kim, E., and Amdahl, J., 2023, "A Rate and Pressure Dependent Elastoplastic Material Model for Glacial Ice Colliding With Marine Structures," Proceedings of the 9th International Conference on Marine Structures (MARSTRUCT 2023), Gothenburg, Sweden, Apr. 3–5, J. W. Ringsberg and C. Guedes Soares, eds., CRC Press, pp. 597–603.
- [7] Liu, Z., Amdahl, J., and Løset, S., 2011, "Plasticity Based Material Modelling of Ice and Its Application to Ship–Iceberg Impacts," Cold Reg. Sci. Technol., 65(3), pp. 326–334.

- [8] Liu, Z., Amdahl, J., and Løset, S., 2011, "Integrated Numerical Analysis of an Iceberg Collision With a Foreship Structure," Mar. Struct., 24(4), pp. 377–395.
- [9] Liu, Z., Amdahl, J., and Løset, S., 2011, "Integrated Numerical Analysis of Iceberg Collisions With Ship Sides," Proceedings of the International Conference on Port and Ocean Engineering Under Arctic Conditions, POAC11-004.
- [10] Yu, Z., Lu, W., Amdahl, J., and Løset, S., 2021, "Glacial Ice Impacts: Part II: Damage Assessment and Ice-Structure Interactions in Accidental Limit States (ALS)," Mar. Struct., 75, p. 102889.
- [11] Yu, Z., and Amdahl, J., 2021, "A Numerical Solver for Coupled Dynamic Simulation of Glacial Ice Impacts Considering Hydrodynamic-Ice-Structure Interaction," Ocean Eng., 226, p. 108827.
- [12] Gagnon, R. E., and Wang, J., 2012, "Numerical Simulations of a Tanker Collision With a Bergy Bit Incorporating Hydrodynamics, a Validated Ice Model and Damage to the Vessel," Cold Reg. Sci. Technol., 81, pp. 26–35.
- Damage to the Vessel," Cold Reg. Sci. Technol., 81, pp. 26–35.
 [13] Herrnring, H. J., 2023, "Experimental and Numerical Investigation of Brittle Ice Crushing Loads," Ph.D. thesis, Hamburg University of Technology, Hamburg, Germany.
- [14] Müller, F., Böhm, A., Herrnring, H., von Bock und Polach, R. U. F., and Ehlers, S., 2023, "Experimental and Numerical Analysis of Ice Crushing Tests With Different Shaped Ice Specimens," International Conference on Offshore Mechanics and Arctic Engineering, Melbourne, Australia, June 11–16, Vol. 86885, American Society of Mechanical Engineers, p. V006T07A015.
- [15] Müller, F., Böhm, A., Herrnring, H., and Ehlers, S., 2024, "Influence of the Ice Shape on Ice-Structure Impact Loads," Cold Reg. Sci. Technol., 221, p. 104175.
- [16] Müller, F., von Bock und Polach, F., and Ehlers, S., 2024, "The Influence of Structural Stiffness and Ice Shape on Impact Loads in Ice-Structure Interaction Experiments," International Conference on Offshore Mechanics and Arctic Engineering, Singapore, June 9–14, Vol. 87844, American Society of Mechanical Engineers, p. V006T07A014.
- [17] Ritch, R., Frederking, R., Johnston, M., Browne, R., and Ralph, F., 2008, "Local Ice Pressures Measured on a Strain Gauge Panel During the CCGS Terry Fox Bergy Bit Impact Study," Cold Reg. Sci. Technol., 52(1), pp. 29–49.
- [18] Töns, T., Ralph, F., Ehlers, S., and Jordaan, I. J., 2015, "Probabilistic Design Load Method for the Northern Sea Route," International Conference on Offshore Mechanics and Arctic Engineering, Newfoundland, Canada, May 31– June 5, Vol. 56567, American Society of Mechanical Engineers, p. V008T07A008.
- [19] Bobeldijk, M. P., 2022, "Polar Bear: On the FEA Model for Simulations for the Design of the Arctic Trials," The Netherlands Organization for Scientific Research, Delft, Technical Report No. TNO Memorandum TNO-2022-MEM-100346896.
- [20] Riska, K., Uto, S., and Tuhkuri, J., 2002, "Pressure Distribution and Response of Multiplate Panels Under Ice Loading," Cold Reg. Sci. Technol., 34(3), pp. 209– 225.